

# Shape analysis based on medial models incorporating object variability

Martin Styner, Guido Gerig

*Dept. of Computer Science, Univ. of North Carolina, Chapel Hill NC 27599, USA*

Jun 01, 2000

## **Abstract.**

Knowledge about the biological variability of anatomical objects is essential for statistical shape analysis and discrimination between healthy and pathological structures. This paper describes a novel approach that incorporates variability of an object population into the generation of a characteristic 3D shape model. The proposed shape representation is a coarse-scale sampled medial description derived from a fine-scale spherical harmonics (SPHARM) boundary description. This medial description is composed of a net of medial samples (m-rep) with fixed graph properties. The medial model is computed automatically from a predefined shape space using pruned 3D Voronoi skeletons to determine the stable medial branching topology. An intrinsic coordinate system and an implicit correspondence between shapes is defined on the medial manifold. Our novel representation describes shape and shape changes in a natural and intuitive fashion. Several studies of biological structures are presented. A new medial shape similarity study of group differences between Monozygotic and Dizygotic twins in lateral ventricle shape demonstrates the meaningful and powerful representation of local and global form.

**Keywords:** Medical Image Analysis, Shape Analysis, Voronoi Skeleton, Medial Shape Description, Brain Morphometry

## 1. Introduction

Quantitative morphologic assessment of individual brain structures in neuroimaging most often includes segmentation followed by volume measurements. Volume changes are intuitive features as they might explain atrophy or dilation of structures due to illness. On the other hand, structural changes like bending/flattening or changes focused at a specific location of a structure, for example thickening of the occipital horn of ventricles, are not sufficiently reflected in global volume measurements. Development of new methods for three-dimensional shape analysis incorporating information about statistical biological variability aims at tackling this issue. Representation and analysis of shape is a complex and challenging problem. It has been argued that a generally applicable solution is not possible and that specific shape descriptions have to be established. In this paper, we present a novel framework for building shape models to be used for shape analysis of anatomical structures.

(Davatzikos et al., 1996) proposed an analysis of shape morphometry via a spatially normalizing elastic transformation. Inter-subject comparisons were made by comparing the individual transformations. The method is applied in 2D to a population of corpora callosa. A similar approach in 3D has been chosen in (Joshi et al., 1997) to compare hippocampi. Using the viscous fluid transformation proposed by Miller (Christensen et al., 1994), inter-subject comparisons were made by analyzing the transformation fields. The *analysis* of transformation fields in both methods has to cope with the high dimensionality of the transformation and the sensitivity to the initial position. Although the number of subjects in the studied populations is low, both show a relatively stable extraction of shape changes (Csernansky et al., 1998). Thompson also uses a non-rigidly transformation to detect sulcal variability and morphological changes to study normal brain development (Thompson et al., 2000a) and diseases specific changes (Thompson et al., 2000b).

The approach taken by (Kelemen et al., 1999) evaluates a population of 3D hippocampal shapes based on a boundary description by spherical harmonic basis functions (SPHARM), which was proposed in (Brechtbühler et al., 1995). The SPHARM shape description delivers a correspondence between shapes on the boundary, which is used in the statistical analysis. As in the approaches discussed before, this approach has to handle the problem of high dimensional features versus a low

number of samples. Further, the detected shape changes are expressed as changes of coefficients that are hard to interpret.

(Golland et al., 1999) in 2D and (Pizer et al., 1999) in 3D proposed two different approaches of applying shape analysis to a medial shape description. (Blum, 1967) claims that medial descriptions are based on the idea of a biological growth model and a 'natural geometry for biological shape.' The medial axis in 2D captures shape intuitively and can be related to human vision (Burbeck et al., 1996; Siddiqi et al., 1997). Both Pizer and Golland propose a sampled medial model that is fitted to individual shapes. By holding the topology of the model fixed, an implicit correspondence between shapes is given and statistical shape analysis can directly be applied.

(Giblin and Kimia, 2000) have proposed a medial hypergraph in 3D. They showed that the hypergraph completely characterizes the shape of an object. Similar to work in 2D by (Siddiqi et al., 1999), this hypergraph could be used for shape recognition and shape design. To our knowledge, no studies have been done towards using the medial graph/hypergraph directly for shape analysis.

In this paper we present a new approach to shape analysis using medial descriptions. The medial description is computed automatically from a population of objects described by their boundaries. The topology of the medial description is calculated by studying the topological

changes of pruned 3D Voronoi skeletons. Voronoi skeletons as a shape representations have been studied intensively in past. The most influential pruning related studies in regard to this work have been performed by (Ogniewicz and Ilg, 1992), Naef (Näf, 1996) and Attali (Attali et al., 1997).

This paper is organized as follows. In the next section, the motivation of our work is discussed guided by an example. Then, we discuss our methods to generate a stable sampled medial description automatically from a population of objects. We start with a general description of the scheme and discuss shape space, common medial branching topology and minimal sampling in detail. In the result section, several neuroimaging applications of medial shape analysis are presented.

## **2. Motivation: Shape analysis in an asymmetry study**

This section describes an example of the intuitive description of shape changes that is inherent to the medial description. We will show an analysis of left/right asymmetry in hippocampi, a subcortical human brain structure which is a structure of interest in schizophrenia research. Asymmetry is defined via the interhemispheric plane, therefore

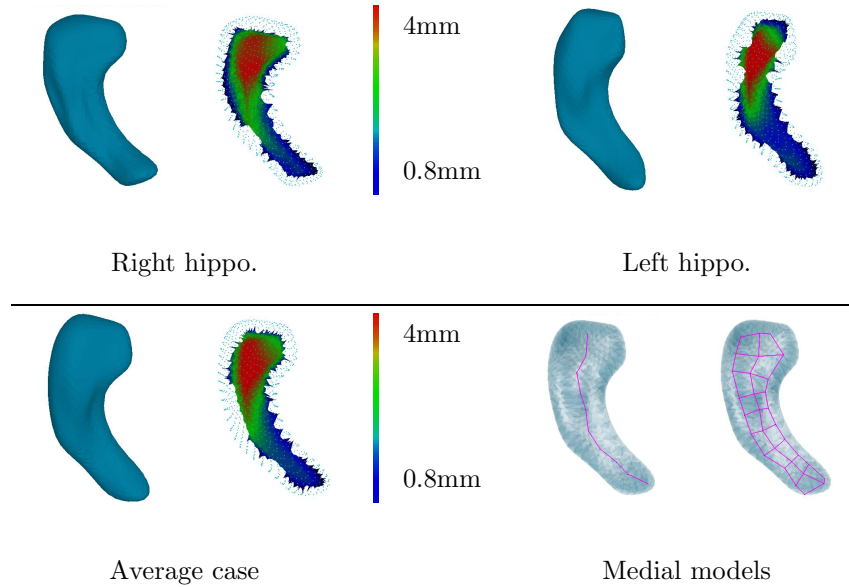


*Figure 1.* Visualization of a left/right hippocampus pair with its average structure. Boundary (left), pruned Voronoi skeleton (right) with thickness coloring (same range for all objects). For the average case the medial axis and grid is shown on the top row.

the right hippocampus was mirrored at this plane for comparison. The main advantage of medial descriptions is the separation of the local shape properties *thickness* and *position*. In the presented case we chose to investigate mainly the thickness information of the medial manifold.

In Fig. 1 the hippocampi are visualized and asymmetry is clearly visible. Volume and medial axis length measurements indicate the same result that the right hippocampus is larger than the left:  $vol_{right} = 2184mm^3$ ,  $vol_{left} = 2023mm^3$ ;  $axis_{right} = 65.7mm$ ,  $axis_{left} = 64.5mm$ . But these measurements do not provide a localization of the detected

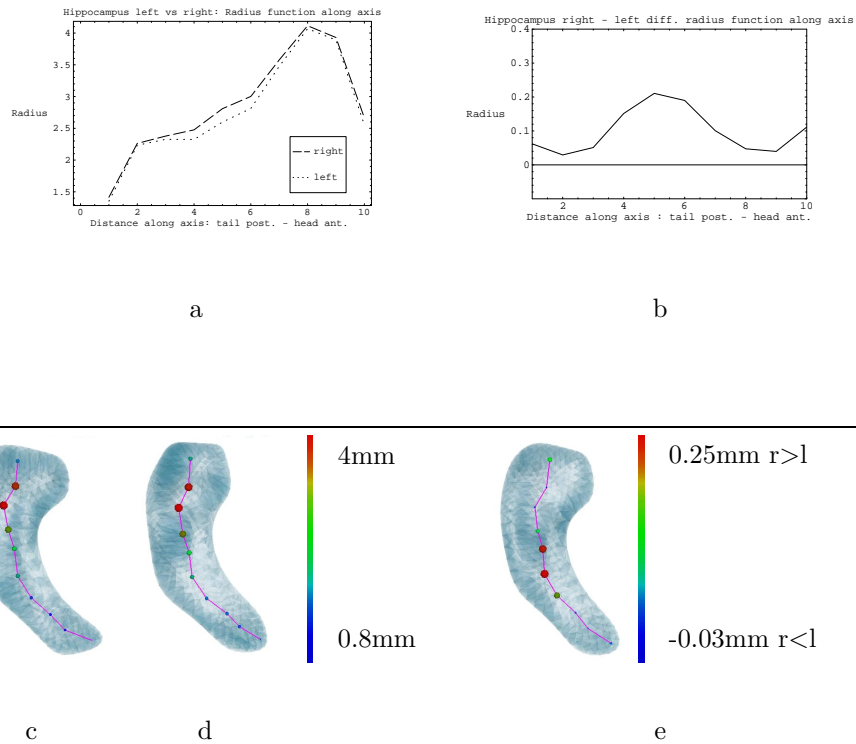
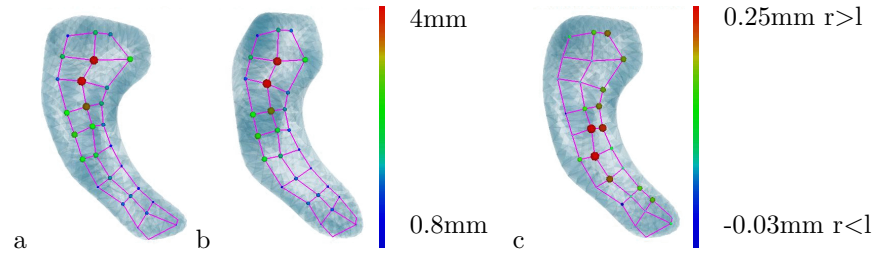


Figure 2. Thickness asymmetry along medial axis (tail to head): a: Radius plot. b: Difference Plot:  $\vec{r}_{right} - \vec{r}_{left}$ . c,d: m-rep description (c: left, d: right). e: Difference  $(R - L)$  at medial atoms with proportional radius/color:  $r \sim |R - L|$ ;  $col \sim (R - L)$ .

asymmetry. This asymmetry can easily be computed and intuitively visualized using our medial description.

When analyzing the thickness of the hippocampi along the medial axis (the intrinsic coordinate system), we get a more localized understanding of the asymmetry. In Fig. 2 the right hippocampus is thicker over the full length of the axis, and the difference is most pronounced in



*Figure 3.* Thickness asymmetry for a left/right hippocampus pair: a,b: M-rep descriptions (a: right, b: left). Radius/color are proportional to the corresponding radius. c: Difference ( $R - L$ ) at medial atoms with proportional radius/color:  $r \sim |R - L|$ ;  $col \sim (R - L)$ .

the middle part of the axis. In order to relate this thickness information with the appropriate location, we visualize it in the medial samples itself. Each medial atom (sample of the medial surface) is displayed by a sphere of size and color that is proportional to its thickness. This kind of display can also be used to visualize the thickness difference of corresponding locations in the right and left hippocampus. The sphere radius and color is proportional to the difference:  $r \sim |R - L|$ ;  $col \sim (R - L)$  (see Fig. 2).

As a next step, we take into account a grid of medial atoms and perform the same analysis as for the axis (see Fig. 3). We observe that the right shape is thicker, but the difference is most pronounced in the middle part.

All parts of the processing are described in the methods section. The applied methods computed the medial branching topology of one single sheet with volumetric overlap larger than 98% and approximation error  $E_{pop}$  less than 0.05.

In the presented hippocampus study the medial description gives a better understanding of the observed asymmetry than simple measurements like volume or even the length of the medial axis. Limiting ourselves to a coarse scale description does not lessen the power of the analysis and asymmetry can reliably be detected and localized.

### 3. Model building methods

The main problem for a medial shape analysis is the determination of a stable medial model in the presence of biological shape variability. Given a population of similar objects, how can we automatically compute a stable medial model? The following sections describe the scheme that we developed to construct a medial *m-rep* model from a population of objects described by boundary parameterization using *spherical harmonics* (*SPHARM*). More details of the scheme are described in (Styner and Gerig, 2001a).

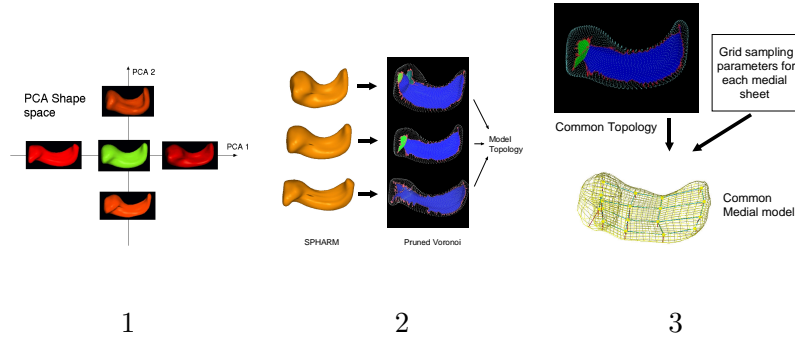


*Figure 4.* Computation of a m-rep model from an object population. 1. Shape space definition. 2. Common medial branching computation. 3. Minimal sampling computation.

In overview, our scheme is subdivided into 3 steps as visualized in Fig. 4. We first define a shape space using Principal Component Analysis. From this shape space we generate the medial model in two steps. First we compute the common branching topology using pruned Voronoi skeletons. Then the minimal sampling of the m-rep model is computed given a maximal approximation error in the shape space.

**M-rep models.** A m-rep (Pizer et al., 1999) is a linked set of medial primitives called medial atoms,  $m = (x, r, \underline{F}, \theta)$ . The atoms are formed from two equal length vectors and are composed of 1) a position  $x$ , 2) a width  $r$ , 3) a frame  $\underline{F}$  implying the tangent plane to the medial manifold and 4) an object angle  $\theta$ . The medial atoms are grouped into figures connected via inter-figural links. These figures are defined as non-branching medial sheets and together form the medial branching

topology. A figure is formed by a set of medial atoms connected by intra-figural links. The connections of the medial atoms and the figures form a graph called 'medial graph' with edges representing either inter- or intra-figural links.

**SPHARM** The SPHARM description is a parametric surface description that can only represent objects of spherical topology (Brechtbühler, 1995). The basis functions of the parameterized surface are spherical harmonics. SPHARM can be used to express shape deformations (Kelemen et al., 1999), and is a smooth, accurate fine-scale shape representation, given a sufficiently small approximation error. Based on a uniform icosahedron-subdivision of the spherical parameterization, we obtain a Point Distribution Model (PDM) directly from the coefficients via a linear mapping. Correspondence of SPHARM is determined by normalizing the parameterization to the first order ellipsoid.

### 3.1. SHAPE SPACE

As a first step in our scheme, we compute a shape space using Principal Component Analysis (PCA) of parametrized objects from a training population. The shape space smoothes the shape variability in the training population, thus making the computations of our scheme more stable. We assume that the shape space is an appropriate representation

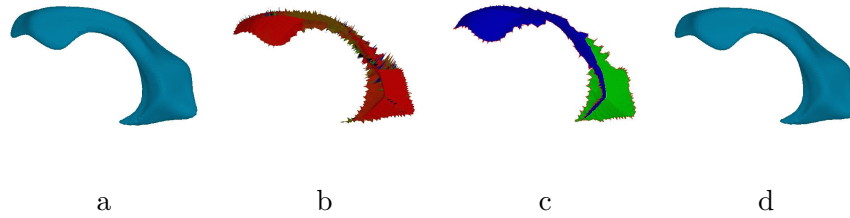


*Figure 5.* Voronoi skeleton pruning scheme applied to a lateral ventricle (side views). a. Original ventricle. b. Original Voronoi skeleton ( $\sim 1600$  sheets). d. Pruned skeleton (2 sheets). c: Reconstruction from pruned skeleton ( $E_{overlap} = 98.3\%$ ).

of the object's biological variability. PCA is computed from SPHARM objects as described by (Kelemen et al., 1999) resulting in the average coefficient vector and the eigenmodes of deformation. The bases of the shape space are the first eigenmodes that cover at least 95% of the population's variability.

A discrete description of the shape space is gained by sampling it either uniformly or probabilistically. These samples form an object set that is a representative sampling of the shape space. All subsequent computations of the model building are then applied to this object set.

### 3.2. COMPUTING A COMMON MEDIAL BRANCHING TOPOLOGY

**Branching topology of a single shape** - The branching topology for a single shape is derived via Voronoi skeletons from finely sampled PDM's. A face-grouping/merging algorithm was developed that groups

the Voronoi faces into a set of medial sheets. The medial sheets are weighted by their volumetric contribution to the overall object volume:

$C_{sheet} = (vol_{skel} - vol_{skel \setminus sheet_i}) / vol_{skel}$ . The sheets are then pruned using a topology preserving deletion scheme.

Our experiments show that a considerable reduction of the number of medial sheets is possible with sacrificing only little accuracy of the reconstruction. In fact, the pruned skeletons of *all* objects studied so far had a volumetric overlap with the original object of more than 98% (see Fig. 5).

**Computation of a common branching topology** - (August et al., 1999) and (Siddiqi et al., 1999) showed that the 2D medial branching topology is quite unstable. In 3D, the medial branching topology is even more unstable. Thus, we developed a matching algorithm that is not based on graph matching but on spatial correspondence.

All objects to be compared are mapped into a common spatial frame by a warped thin plate splines registration based on the correspondence established by the SPHARM description. In order to minimize the mapping distortions, the average object of the shape space is chosen to provide the common spatial frame. The common branching topology is then computed iteratively starting with the topology of the average object as the initial guess. Non-corresponding sheets are identified using the paired Mahalanobis distance between sheet centers. These

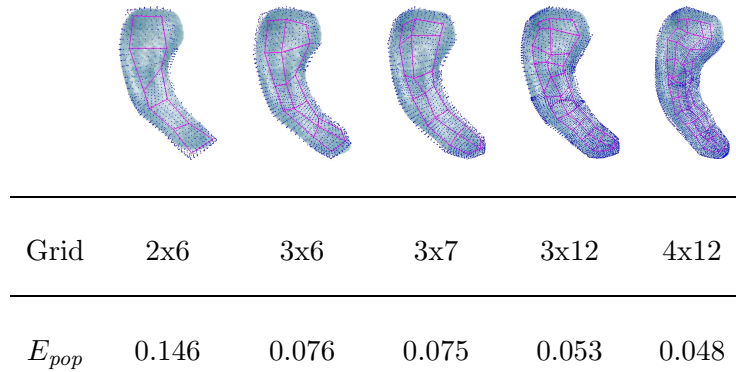


Figure 6. Sampling approximation errors  $E_{pop}$  of the m-rep implied surface (dark blue dots) with the original object boundary (light blue transparent) in a hippocampus structure ( $r_{avg} = 2.67$  mm). The m-rep grids are visualized as red lines. The grid dimensions are shown in the second row, and the  $E_{pop}$  errors in the third row.

non-corresponding sheets are added to the current branching topology. Every sheet of all objects in the shape space is matched by at least one sheet in the final common branching topology.

### 3.3. MINIMAL SAMPLING OF M-REP MODEL

From the common branching topology we compute the sampling of the associated sheets by a grid of medial atoms. The m-rep model is determined by the common branching topology and a set of parameters that specify the grid dimensions for each sheet. The sampling algorithm is based on the longest 1D thinning axis of the edge-smoothed 3D medial sheet. The set of grid parameters is optimized to be minimal while the

corresponding m-rep deforms into every object in the shape space with a predefined maximal approximation error. The approximation error is computed as Mean Absolute Distance ( $MAD$ ) of the implied and the original boundary. In order to have an error independent of the object size, we normalize with the average radius of all skeletons in the population:  $E_{pop} = MAD/r_{avg,pop}$ . In Fig. 6 we show the error of various sampling parameters. The limiting error is chosen in the range of 5% to 10% depending on the structure.

#### 3.4. DEFORMING THE M-REP MODEL INTO AN INDIVIDUAL SHAPE

Once a m-rep model is computed, we want to fit it into individual shapes. This fit is done in two steps. First we obtain a good initial estimate which is then refined in a second step to fit to the boundary. The initial estimate is obtained by warping the m-rep model from the common frame into the frame of the individual shape using the SPHARM correspondence on the boundary. From that position we run an optimization that changes the features of the m-rep atoms to improve the fit to the boundary as described in (Joshi et al., 2001). Local similarity transformations as well as rotations of the local angulation are applied to the medial atoms. The fit to the boundary is constrained

by an neighborhood dependent prior that guarantees the smoothness of the medial manifold.

#### 4. Object alignment and scaling

As a prerequisite for any shape analysis and shape similarity calculation, shapes have to be normalized with respect to a reference coordinate frame. Since we are interested in measuring shape differences, a normalization is needed to eliminate differences that are due to rotation, translation and magnification. Normalization of translation and rotation is accomplished by aligning the objects via the first order ellipsoid. This perfectly matches center and axes of the first order ellipsoids (see Fig. 7).

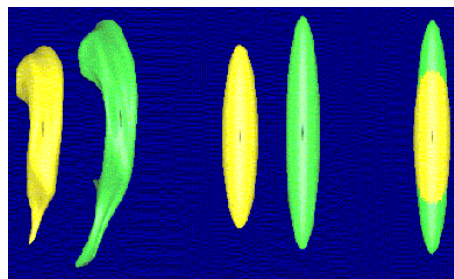


*Figure 7.* Object alignment. Two left lateral ventricles are aligned to perfectly match the center and axis of the first order ellipsoid; left: objects, middle: first order ellipsoids, right: aligned ellipsoids.

In order to normalize for magnification, an appropriate scaling method has to be defined. The choice of the scaling method depends on the task and the type of objects. We investigated two possibilities (see also Fig. 8):

- A No scaling correction: The computation of shape differences without any scale normalization reveals differences between small and large objects even though they might have the same shape properties. Thus, the differences will reflect mixed values of both the shape differences and the size differences.
- B Uniform scaling to unit volume: Creating a shape difference measure that is orthogonal in its nature to the volume measure has the potential to reveal information additional to size. The volume measurements can be incorporated later into a multivariate statistical analysis as an additional orthogonal feature.

## 5. M-rep shape analysis

The main advantage of a medial shape analysis over a boundary shape analysis is the separation of the two medial shape properties of local position and thickness. Fig. 9 demonstrates how thickness and

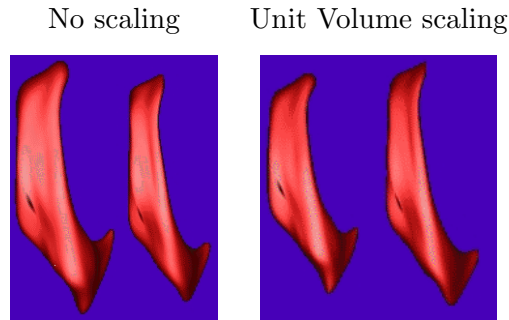


*Figure 8.* Object scaling. Pairs of right lateral ventricles (MZ twin pair) unscaled (left) and scaled to unit volume (right). This example shows that shapes are quite similar and that the scaling corrected for an existing size difference.

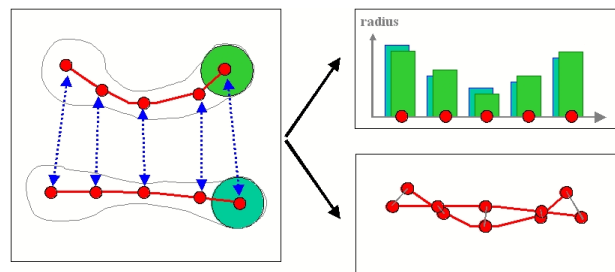


*Figure 9.* Medial shape analysis (schematically shown in 2D): The differences in the thickness and position properties between 2 m-reps can be studied separately. The properties express different kinds of underlying processes (growth vs. deformation).

position capture different forms of shape deformation, i.e. thickness changes are due to locally uniform growth forces and positional changes are due to locally deformation forces. Since these two features are quasi-orthogonal, we investigate them separately, which lends additional statistical power to our analysis.

When computing group differences instead of pair-wise differences, we designate the average medial description of all groups to be the reference object. Our medial shape analysis computes for each subject the difference to this reference object. In this paper, the presented group study involve pair-wise differences, thus there was no need for a reference object.

We can perform a global and a local shape analysis using the m-rep description. In the global analysis, we integrate the properties over all atoms of the whole m-rep to compute a one position and one thickness feature per m-rep. In the local analysis, we study each atom's properties individually to detect locations of significant differences. In this paper, we treat the atoms to be independent of each other. This viewpoint is not fully accurate, but appropriate for a preliminary analysis.

## 6. Applications

### 6.1. MEDIAL MODEL COMPUTATION

The scheme has been applied to different studies with populations of several human brain structures; the overall number of processed cases is shown in parenthesis: hippocampus-amygdala (60 cases), hippocam-

pus (200), thalamus (56), pallide globe (56), putamen (56) and lateral ventricles (80). The computed models are shown in Figs. 10 and 11. Three of the model building studies are presented in more detail in the following paragraphs.

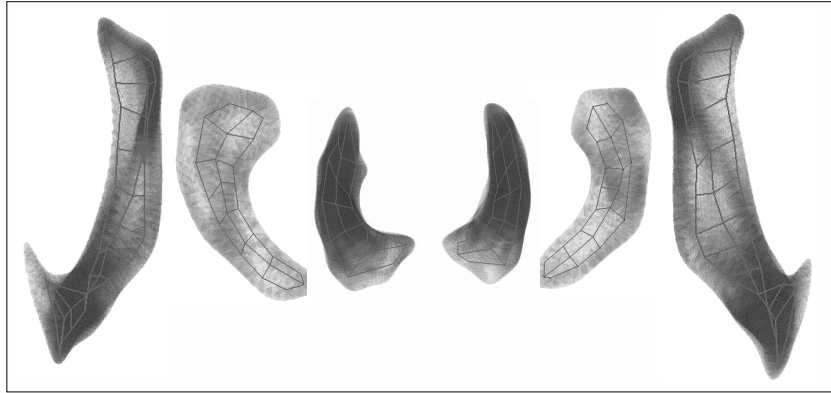


*Figure 10.* Selection of medial models of anatomical structures in the left and right brain hemisphere. All of these models are single-figure models. From outside to inside: lateral ventricle, hippocampus, pallide globe.

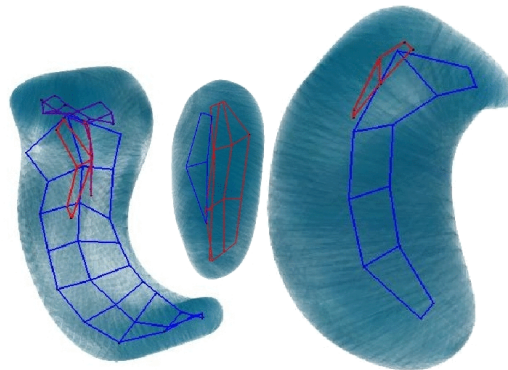


*Figure 11.* Selection of medial models of anatomical brain structures. All of these models are multi-figure models. From left to right: hippocampus-amygdala complex, pallide globe and thalamus.

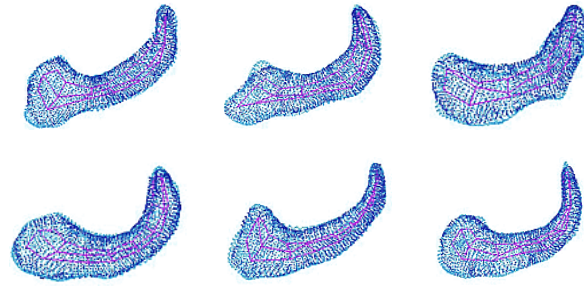


*Figure 12.* Six individual m-rep descriptions of the hippocampus study. The visualizations show m-rep grids as red lines, the m-rep implied surface as dark blue dots and the original object boundary in transparent light blue.

**Hippocampus schizophrenia study.** The hippocampus structure of an object population with schizophrenic patients (56 cases) and healthy controls (26 cases) is investigated. The goal of the study was to assess shape asymmetry between left and right side objects, and also to analyze shape similarity between patients and controls. The model was built on a object population that included the objects of all subjects on both sides, with the right hippocampi mirrored at the interhemispheric plane prior to the model generation.

The SPHARM coefficients were normalized for rotation and translation using the first order ellipsoid. The size was normalized to unit volume. The shape space was defined by the first 13 eigenmodes with every other eigenmode holding less than 1% of the variability in the population. All objects in the shape space had a medial branching topology of a single medial sheet with a volumetric overlap of more than

98%. Thus, the common topology was a single sheet. The computed minimal grid sampling of  $3 \times 8$  had an  $E_{pop}$  error of less than 5% for all objects in the shape space. The application of this model to the whole hippocampus population of 164 objects generated  $E_{pop}$  errors in the range of  $[0.048 \dots 0.088]$  with an average error of 0.058 (see Fig. 12). The average radius is 3.0 mm and thus the average error is 0.17mm. The original sampling is  $0.94^2 \times 1.5$ mm, and thus the individual m-reps are computed with sub-voxel accuracy.

**Lateral ventricle twin study.** Another study investigates the lateral ventricle structure in a population of 10 monozygotic and 10 dizygotic twins. The same processing has been performed as in the first study. The SPHARM coefficients were normalized for rotation and translation using the first order ellipsoid. The size was normalized to unit volume. The first 8 eigenmodes define the shape space, which holds 96% of the variability of the population. The medial branching topologies in the object set varied between one to three medial sheets with an volumetric overlap of more than 98% for each object. The single medial sheet topology of the average object matched all sheets in the common frame since the matching algorithm allows one-to-many matches. Thus, the common medial topology was computed to be a single sheet. The minimal sampling of the medial topology was computed with a maximal  $E_{pop} \leq 0.10$  in the shape space. The application of this model to the

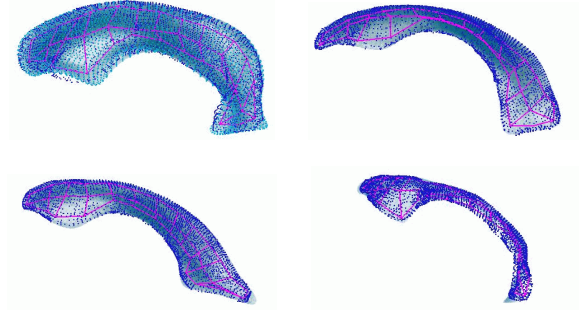


*Figure 13.* Four individual m-rep descriptions of the lateral ventricle study. The visualizations show m-rep grids as red lines, the m-rep implied surface as dark blue dots and the original object boundary in transparent light blue.

whole population generated  $E_{pop}$  errors in the range of  $[0.057 \dots 0.15]$  with an average error of 0.094 (see Fig. 13). The average radius is 2.26mm and thus the average error is 0.21mm.

**Hippocampus-amygdala schizophrenia study.** This section presents our scheme applied to a hippocampus-amygdala population from a schizophrenia study (30 subjects). As in the first study, shape asymmetry and similarity analysis are to be determined and thus the same processing has been performed. The SPHARM coefficients were determined and normalized regarding rotation and translation using the first order ellipsoid. The scale was normalized to unit volume. The shape space is defined by the first 6 eigenmodes which cover 97% of the variability in the population. The medial branching topologies in the object set varied between two to five medial sheets with an volumetric

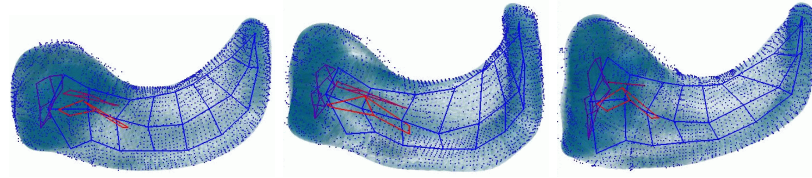


*Figure 14.* Three m-rep descriptions of the hippocampus-amygdala study. The visualizations show m-rep grids as colored lines, the m-rep implied surface as dark blue dots and the original object boundary in transparent light blue.

overlap of more than 98% for each object. The common branching topology was computed to be composed of four sheets. The minimal sampling of the medial topology was computed with a maximal  $E_{pop} \leq 0.10$  in the shape space. The application of this model to the whole population generated  $E_{pop}$  errors in the range of  $[0.035 \dots 0.112]$  with an average error of 0.084 (see Fig. 14). The average radius is 3.6mm and thus the average error is 0.30mm.

## 6.2. SHAPE ANALYSIS FOR GROUP DIFFERENCE

The lateral ventricle study presented before is investigated for group differences between Monozygotic (MZ, 5 pairs) twins, Dizygotic (DZ, 5 pairs) twins and unrelated (NR, 10 pairs) subject pairs. All groups are gender, age and handedness matched. The lateral ventricle is a fluid filled structure in the center of the human brain that is divided into a left and a right part located in the respective brain hemispheres (see

Fig. 6.2). The original brain images were provided by D. Weinberger, NIMH Neuroscience in Bethesda, Maryland. The segmentation method used a single gradient-echo channel (T1w, matrix 256x256x128, resolution 0.9375<sup>2</sup>x1.5mm) with manual seeding for Parzen-window based non-parametric supervised statistical classification. Manually-guided three-dimensional connectivity was used to extract the left and right lateral ventricles. The segmented structures were postprocessed using a morphological closing operation to provided simply connected 3D objects.

In this study, we were mainly interested in investigating the degree of similarity of the lateral ventricles between subject pairs. Thus, the goal of the study was to determine whether MZ twins have more similarly shaped lateral ventricles than DZ twins or unrelated (NR) subject pairs. The population size of each group is very small, so the observed effect must be quite large for the statistical analysis to yield a significant result. A previous study was performed by Bartley et al (Bartley et al., 1997) on the same datasets with the goal of distinguishing the groups. They compared cortical gyral patterns and the total brain volumes. Both measures showed significant differences between the MZ and DZ groups.

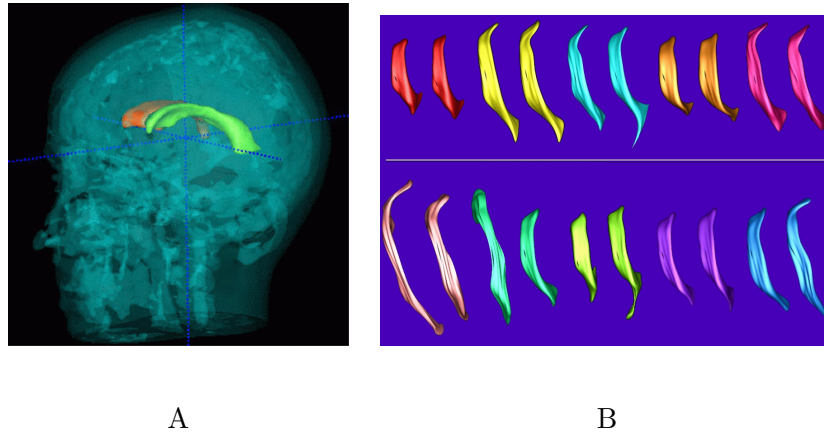


*Figure 15.* A: Three-dimensional rendering of the skin and bone structures of one subject's head (transparent) and the lateral ventricles. B: Visualization of the right-side lateral ventricles of all twin pairs (top view, same color for pairs) scaled to unit volume. Top row: MZ twins. Bottom Row: DZ twins.

### 6.2.1. Volume similarity analysis

We studied each twin pair's similarity using the normalized absolute volume difference:  $\Delta vol_{T_{1,2}} = |vol_{T_1} - vol_{T_2}| / (vol_{T_1} + vol_{T_2})$ . As shown in Fig. 16, there is a trend in both brain hemispheres between the two groups, but no significant conclusions can be drawn since the volume measurement distributions are overlapping. The  $p$ -value for discriminating the two groups is at 0.15/0.16, which is non-significant at a 5% significance level (see Tab. I).

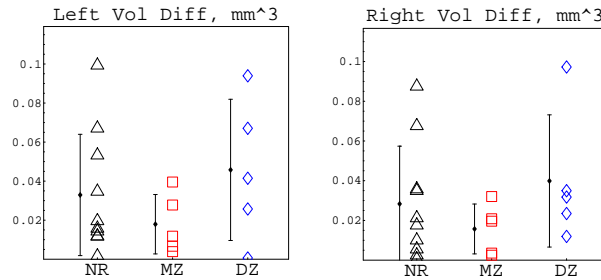
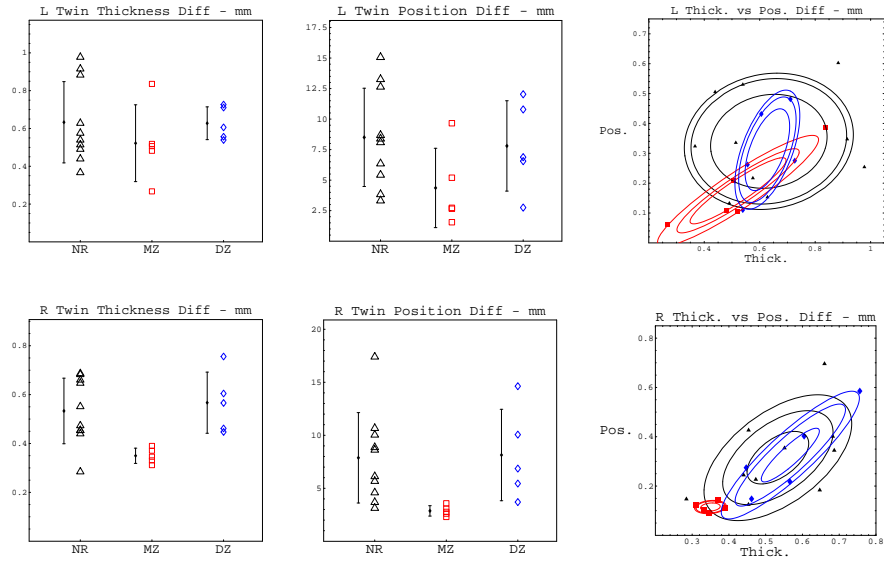


Figure 16. Plot of pairwise relative ventricle volume difference  $\Delta vol_{T_{1,2}}$  between MZ and DZ twin groups. Results of left and right ventricles are shown in the left and right figures. No significant conclusions can be drawn.

### 6.2.2. Medial shape similarity analysis

The medial shape analysis is performed on the objects that have been normalized to unit volume. The goal of the medial shape analysis is to detect global shape differences and also to pinpoint the locations of significant group difference in a atom-by-atom shape analysis. These differences can manifest in the medial properties of thickness and position (see section 5), each of them potentially at different locations.

In the global m-rep shape analysis, we integrate the local differences between corresponding atoms. Each of the two m-rep properties detects a higher level of similarity between MZ twins than between DZ twins at a significant p-value (5% significance level) on the right side (see Fig. 17, Tab. I). No significance can be detected on the left side. When studying the joined feature space of both thickness and position differences, this becomes even better visible. Furthermore, when comparing



*Figure 17.* Medial shape analysis plots of pairwise shape differences of the thickness (1. column) and position (2. column) property. In the 3. column a combined analysis is shown, which displays the quartile ellipsoids of the 3 groups (MZ=red squares, DZ=blue diamonds, NR=black triangles). Top row: left ventricle, bottom row: right ventricle. It is clearly visible that the effect is much stronger on the right side than on the left.

the MZ group to the population of non-related pairs, we observe that the similarity in MZ twins significantly differs from the similarity of non-related pairs. This is not the case for the dizygotic twin pairs, thus suggesting that there isn't a difference that can be detected with our methods. We also computed a global boundary shape analysis (Styner and Gerig, 2001b) using the SPHARM description, which had the same

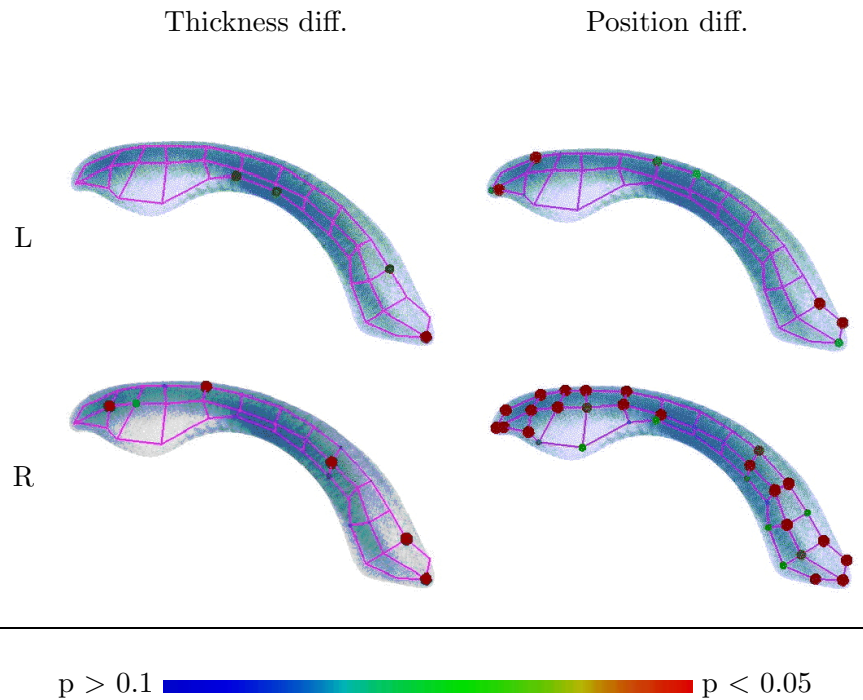
outcome as the medial analysis, but had slightly different p-value's from the analysis.

Table I. Table of  $p$ -values for group mean difference testing between MZ and DZ twin pairs and unrelated pairs. Bold numbers are significant at 5% significance level.

	MZ/DZ	MZ/Other	DZ/Other
Volume diff - Left	0.151	0.333	0.486
M-rep global thickness diff - Left	0.316	0.356	0.959
M-rep global position diff - Left	0.157	0.068	0.75
Volume diff - Right	0.167	0.377	0.500
M-rep global thickness diff - Right	<b>0.016</b>	<b>0.011</b>	0.646
M-rep global position diff - Right	<b>0.026</b>	<b>0.005</b>	0.91

The local medial shape analysis is visualized in Fig. 18 by indicating location of significant group differences between MZ and DZ twins. These locations are not the same for the thickness and position features. As in the global analysis, the right side shows a much larger effect than the left side. It is also clearly visible that the locations of significant difference cluster in the posterior and anterior part on the *position* analysis. This suggests that the main shape difference between MZ and DZ twin pairs in this study is that MZ twin pairs have less deformation

differences in the posterior and anterior part of the lateral ventricle than DZ twin pairs.



*Figure 18.* Local medial shape analysis of MZ vs. DZ twin pairs. Lateral ventricles shown in side view. The radius of the medial atoms is proportional to the significance of the group difference at its location of either the thickness or position property. A clustering in the anterior and posterior part is visible in the right side position analysis (bottom right).

The results of the medial shape analysis reveals interesting new information about the structure of brain ventricles in genetically identical MZ twin pairs, non-identical DZ twins, and non-related but age and gender matched pairs. We are well aware that we have to be cautious

with conclusions due to the small sample size. The size normalized right ventricles reveal that MZ twin pairs show a very small shape difference, with low variability, suggesting that the shapes after normalization are very similar. Surprisingly, this strong and significant effect is not found in the left ventricles, where there is only a trend indicating more similar ventricle shape in MZ as compared to DZ. The statistics further illustrates that DZ twin pairs didn't differ from unrelated pairs in our analysis.

## 7. Summary and Conclusions

We present a new approach to the description and analysis of shape for objects in the presence of biological variability. The proposed description is a medial description derived from a boundary description. The generation of the medial description takes into account the biological variability of a set of training shapes, which is a novel concept and a step further towards a natural shape representation. We have shown that we can compute a stable medial description for a population of shapes. Using the medial description we can visualize and quantitate globally and locally computed shape features regarding similarity. Since

a correspondence is given on the medial manifold a statistical analysis can be directly applied.

The choice of a *fixed* m-rep topology has several advantages, e.g. enabling an implicit correspondence for statistical analysis. On the other hand, a fixed topology m-rep model cannot precisely capture the topology of an individual object. The determined m-rep is therefore always an approximation of the object.

The SPHARM boundary correspondence has shown to be a good approach in the general case, but it has inherent problems e.g. in case of rotational symmetry. Although not used in our correspondence scheme, externally computed correspondences can be included into the scheme.

The MZ/DZ twin study demonstrates that shape measures reveal new information additional to size measurements which might be relevant for improved understanding of structural differences in normal populations but also in comparisons between healthy control groups and patients. Twin studies offer the advantage to reduce natural biological variability by choosing subjects with identical genes. Our twin study clearly demonstrates that significant differences between MZ and DZ pairs could not be found by volume measurements but only by shape analysis. There is a significant group difference between MZ and DZ twin pairs for the right but not for the left ventricle. We have no obvious explanation for this finding but hope to get more insight through close

collaboration with experts in neurobiology and neurodevelopment. A follow-up study currently analyzes differences between MZ twins discordant for schizophrenia to reveal insight into hypothesized morphologic changes due to illness. Analysis of shape changes similarly to the presented case study might become important in longitudinal assessments of morphologic change due to developmental or degenerative processes.

As next steps, we have to study more thoroughly the robustness of our scheme. Additional applications to clinical studies in Schizophrenia and other neurological diseases are in progress. Also, more sophisticated methods of medial shape analysis are in development as indicated in (Yushkevich and Pizer, 2001).

### **Acknowledgements**

Miranda Chakos and MHNCR image analysis lab at Psychiatry UNC Chapel Hill Hospitals kindly provided the original MR and segmentations of the hippocampi. Ron Kikinis and Martha Shenton, Brigham and Women's Hospital, Harvard Medical School, Boston provided the original MR and segmentations of the amygdala-hippocampus study. We further acknowledge Daniel Weinberger, NIMH Neuroscience in Bethesda for providing the twin datasets that were segmented in the

UNC MHCRC image analysis lab. We are thankful to Christian Brechbühler for providing the software for SPHARM surface parameterization and description. We are further thankful to Steve Pizer, Tom Fletcher and Sarang Joshi of the MIDAG group at UNC for providing us with m-rep tools. We would like to thank Steve Pizer for his insightful comments and discussions about m-rep and other medial shape descriptions. Sarang Joshi is acknowledged for discussions about the m-rep deformation.

## References

- Attali, D., G. Sanniti di Baja, and E. Thiel: 1997, 'Skeleton simplification through non significant branch removal'. *Image Proc. and Comm.* **3**(3-4), 63–72.
- August, J., K. Siddiqi, and S. Zucker: 1999, 'Ligature Instabilities in the Perceptual Organization of Shape'. In: *IEEE Comp. Vision and Pattern Rec.*
- Bartley, A., D. Jones, and D. Weinberger: 1997, 'Genetic variability of human brain size and cortical patterns'. *Brain* **120**, 257–269.
- Blum, T.: 1967, 'A transformation for extracting new descriptors of shape'. In: *Models for the Perception of Speech and Visual Form*. MIT Press.
- Brechbühler, C.: 1995, *Description and Analysis of 3-D Shapes by Parametrization of Closed Surfaces*. Diss., IKT/BIWI, ETH Zürich, ISBN 3-89649-007-9.
- Brechbühler, C., G. Gerig, and O. Kübler: 1995, 'Parametrization of closed surfaces for 3-D shape description'. *CVGIP: Image Under.* **61**, 154–170.
- Burbeck, C., S. Pizer, B. Morse, D. Ariely, G. Zauberaman, and J. Rolland: 1996, 'Linking object boundaries at scale: a common mechanism for size and shape judgements'. *Vision Research* **36**, 361–372.
- Christensen, G., R. Rabbitt, and M. Miller: 1994, '3D brain mapping using a deformable neuroanatomy'. *Physics in Medicine and Biology* **39**, 209–618.
- Csernansky, J., S. Joshi, L. Wang, J. Haller, M. Gado, J. Miller, U. Grenander, and M. Miller: 1998, 'Hippocampal morphometry in schizophrenia via high dimensional brain mapping'. *Proc. Natl. Acad. Sci. USA* **95**, 11406–11411.
- Davatzikos, C., M. Vaillant, S. Resnick, J. Prince, S. Letovsky, and R. Bryan: 1996, 'A Computerized Method for Morphological Analysis of the Corpus Callosum'. *J. of Comp. Ass. Tomography.* **20**, 88–97.
- Giblin, P. and B. Kimia: 2000, 'A formal classification of 3D medial axis points and their local geometry'. In: *IEEE Comp. Vision and Pattern Rec.* pp. 566–573.

- Golland, P., W. Grimson, and R. Kikinis: 1999, 'Statistical Shape Analysis Using Fixed Topology skeletons: Corpus Callosum Study'. In: *Inf. Proc. in Med. Imaging*. pp. 382–388.
- Joshi, S., M. Miller, and U. Grenander: 1997, 'On the geometry and shape of brain sub-manifolds'. *Pattern Recognition and Artificial Intelligence* **11**, 1317–1343.
- Joshi, S., S. Pizer, T. Fletcher, A. Thall, and G. Tracton: 2001, 'Multi-scale deformable model segmentation based on medial description'. In: *Inf. Proc. in Med. Imaging*.
- Kelemen, A., G. Székely, and G. Gerig: 1999, 'Elastic Model-Based Segmentation of 3D Neuroradiological Data Sets'. *IEEE Trans. Med. Imaging* **18**, 828–839.
- Näf, M.: 1996, 'Voronoi Skeletons: a semicontinuous implementation of the 'Symmetric Axis Transform' in 3D space'. Ph.D. thesis, ETH Zürich, Communication Technology Institute IKT/BIWI.
- Ogniewicz, R. and M. Ilg: 1992, 'Voronoi Skeletons: Theory and Applications'. In: *IEEE Comp. Vision and Pattern Rec.* pp. 63–69.
- Pizer, S., D. Fritsch, P. Yushkevich, V. Johnson, and E. Chaney: 1999, 'Segmentation, Registration, and Measurement of Shape Variation via Image Object Shape'. *IEEE Trans. Med. Imaging* **18**, 851–865.
- Siddiqi, K., A. Ahokoufandeh, S. Dickinson, and S. Zucker: 1999, 'Shock Graphs and Shape Matching'. *Int. J. Computer Vision* **1**(35), 13–32.
- Siddiqi, K., B. Kimia, S. Zucker, and A. Tannenbaum: 1997, 'Shape, Shocks and Wiggles'. *Image and Vision Computing Journal* **17**, 365–373.
- Styner, M. and G. Gerig: 2001a, 'Medial models incorporating shape variability'. In: *Inf. Proc. in Med. Imaging*. pp. 502–516.
- Styner, M. and G. Gerig: 2001b, 'Three-dimensional medial shape representation incorporating object variability'. In: *IEEE Comp. Vision and Pattern Rec.* submitted.
- Thompson, P., J. Giedd, R. Woods, D. MacDonald, A. Evans, and A. Toga: 2000a, 'Growth patterns in the developing brain detected by using continuum mechanical tensor maps'. *Nature* **404**, 190–193.
- Thompson, P., M. Mega, and A. Toga: 2000b, *Brain Mapping: The Disorders*, Chapt. Disease-Specific Brain Atlases. Academic Press.
- Yushkevich, P. and S. Pizer: 2001, 'Coarse to fine shape analysis via medial models'. In: *Inf. Proc. in Med. Imaging*.

